Letter

Spin dynamics study and experimental realization of tunable single-ion anisotropy in multiferroic $Ba_2CoGe_2O_7$ under external magnetic fields

Rajesh Dutta,[1,2,*] Henrik Thoma,[1,2] Igor Radelytskyi,[2] Astrid Schneidewind,[2] Vilmos Kocsis,[3,4,†] Yusuke Tokunaga,[3,5] Yasujiro Taguchi,[3] Yoshinori Tokura,[3,6,7] and Vladimir Hutanu[1,2]

[1]*Institut für Kristallographie, RWTH Aachen Universität, 52066 Aachen, Germany*
[2]*Jülich Centre for Neutron Science at Heinz Maier-Leibnitz Zentrum, 85747 Garching, Germany*
[3]*RIKEN Center for Emergent Matter Science (CEMS), Wako, Saitama 351-0198, Japan*
[4]*Department of Physics, Budapest University of Technology and Economics, and MTA-BME Lendület Magneto-optical Spectroscopy Research Group, 1111 Budapest, Hungary*
[5]*Department of Advanced Materials Science, University of Tokyo, Kashiwa 277-8561, Japan*
[6]*Quantum-Phase Electronics Center, Department of Applied Physics, University of Tokyo, Tokyo 113-8656, Japan*
[7]*Department of Applied Physics, University of Tokyo, Hongo, Tokyo 113-8656, Japan*

(Received 21 December 2020; revised 31 May 2021; accepted 24 June 2021; published 7 July 2021)

We report a spin-wave study on multiferroic $Ba_2CoGe_2O_7$ under magnetic fields up to 12 T using low-energy inelastic neutron scattering. In-plane transverse (T_1) spin-wave modes are highly dispersive along (h00) and rather flat but strong in intensity along (30l). In addition, two dispersive electromagnon modes have been observed around 3.5 meV. Dispersion of the out-of-plane transverse modes (T_2) under fields reveals that the single-ion anisotropy constant decreases with increasing magnetic field, which is consistent with the linear spin-wave theory. Our results imply that the field-dependent single-ion anisotropy plays a crucial role in determining the characteristics of T_2 and electromagnon modes in the three-dimensional anisotropic spin-wave spectrum.

DOI: 10.1103/PhysRevB.104.L020403

Strongly correlated electron systems involving square lattice Heisenberg antiferromagnets (SLHAFs) with spin $\geqslant 1/2$ serve as an upstanding platform to study many exotic quantum phenomena both experimentally and theoretically [1–6]. The emergence of exotic novel quantum phases, under external stimuli, e.g., magnetic or electric field and uniaxial pressure or topological surface effect, are highly intercorrelated depending on the symmetric exchange, single-ion anisotropy (SIA), and Dzyaloshinskii-Moriya (DM) interactions [4,7–11]. Multiferroic $Ba_2CoGe_2O_7$ is one of the intriguing quantum materials exhibiting induced spontaneous electric polarization which was explained by a spin-dependent d-p hybridization mechanism [12–15], but in a collinear staggered antiferromagnetic (AFM) state below the Néel temperature ($T_N = 6.7$ K). As a consequence, both electro- and magnetic-active excitations (electromagnon modes) are expected in the multiferroics state and have been observed around 4 meV in the magnetic excitation spectrum along with conventional magnons using THz spectroscopy and inelastic neutron scattering (INS) [16–20].

However, detailed information about the momentum resolved scattering cross sections $S(Q, w)$ of the spin-wave modes was not possible to obtain using electron spin resonance (ESR), far-infrared (FIR), and circular dichroism THz spectroscopies as they can only probe the zone-center excitations in reciprocal space, like Raman spectroscopy. Also, the previous INS studies of $Ba_2CoGe_2O_7$ [16,18,19] have dealt with only in-plane (a-b) spin dispersion where the applied magnetic fields were limited to 3 T, even far below the field ($H \approx 15$ T) of onset saturation magnetization. In the presence of weak interplane ferromagnetic (FM) exchange interaction, $Ba_2CoGe_2O_7$ has been treated, so far, as quasi-two-dimensional (Q2D) AFM, but there is no single report on spin dispersion along l. As the induced electric polarization can be tuned by an external magnetic field, it is crucial to study the nature of the electromagnons as well as the conventional magnons at relatively high fields in three dimensions, especially when the system exhibits an effective spin anisotropy, i.e., a strong intercorrelation between antisymmetric DM interactions and the SIA under the applied fields. Such interplay, especially between the SIA and the magnetic field, is explored here through experimental findings in multiferroic quantum materials.

In this Letter, we present a detailed INS study of $Ba_2CoGe_2O_7$ under transverse magnetic fields up to 12 T at 4 K and reveal the tunable SIA constant under magnetic fields and the three-dimensional anisotropic nature of spin dispersion. We find that in-plane transverse modes (T_1) of the magnetic l dispersion are stronger than that along the h dispersion, indicating the anisotropic in-plane spin fluctuations. The relatively high-energy electromagnon modes (between 2.5 and 4.5 meV) are seemingly dispersive in 3D also, but slightly robust in the lower magnetic field region. Most interestingly,

*Corresponding author: rajesh.dutta@frm2.tum.de
†Present address: Institut für Festkörperforschung, Leibniz IFW Dresden, 01069 Dresden, Germany.

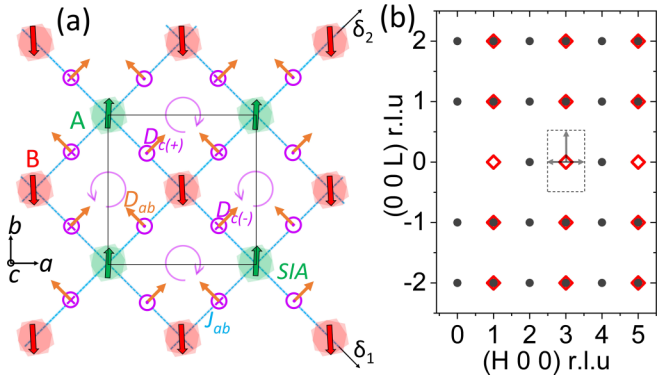

FIG. 1. (a) $Ba_2CoGe_2O_7$ unit cell (black square) projected along the c axis; only the Co^{2+} spins are shown in the sublattices A (green) and B (red) with the in-plane exchange interaction J_{ab} and DM interaction. On each bond, the direction of the i- to j-site is indicated by δ_1 and δ_2. Staggered out-of-plane components of DM interaction $D_{c(+,-)}$ are represented as dotted and crossed pink circles, respectively. Uniform components D_{ab} are shown as orange arrows. Colored filled double hexagons on each Co^{2+} indicate the on-site SIA. (b) Schematic of ($h0l$) reciprocal plane containing both the nuclear (gray dots) and the magnetic (red empty diamonds) reflections. The black dotted rectangle indicates the magnetic Brillouin zone of (300), where the arrows show the positions of the performed constant-Q scans.

our findings on small changes in the SIA constant under a magnetic field indicate that a competition between SIA and Zeeman interaction (external magnetic field) takes place when the SIA is quite strong in the collinear state, thus providing an important insight into the general 2D square lattice AFM in the quantum limit.

An INS experiment on a single crystal of $Ba_2CoGe_2O_7$ grown by the floating zone method [12,13,21,22] was carried out on the cold-neutron triple-axis spectrometer PANDA at Heinz Maier-Leibnitz Zentrum (MLZ) [23]. The sample was aligned with its reciprocal ($h0l$) plane as the horizontal scattering plane. Magnetic fields up to 12 T, using an actively shielded vertical cryomagnet, were applied parallel to the vertical b axis. The measurements were performed using a fixed final energy $E_f = 5.107$ meV of neutrons and the energy resolution at the elastic line was ≈0.16 meV. The incident and final energies were selected via the (002) Bragg reflection of a pyrolithic graphite (PG) monochromator and analyzer with double focusing. A cooled Be filter was mounted before the analyzer to suppress the higher-order neutrons. As shown in Fig. 1, we interpret our results in the orthogonally twinned around c-axis and noncentrosymmetric tetragonal cell ($P\bar{4}2_1m$, lattice parameters $a = b = 8.41$ Å and $c = 5.537$ Å) [12,19,21], with the magnetic wave vector $\mathbf{q} = (1, 0, 0)$.

Figure 2 summarizes the effects of low magnetic fields on the three-dimensional magnetic excitations. Along both the in- and out-of-plane directions, all the constant-Q scans show conventional T_1 and T_2 modes below 2.5 meV in energy and the weak electromagnon (EM) modes above 2.5 meV. Figures 2(b) and 2(d) explicitly show that at the zero field, both the maximum energy and the spin-wave velocity (slope) of the T_1 mode along (30l) are around five times less than that

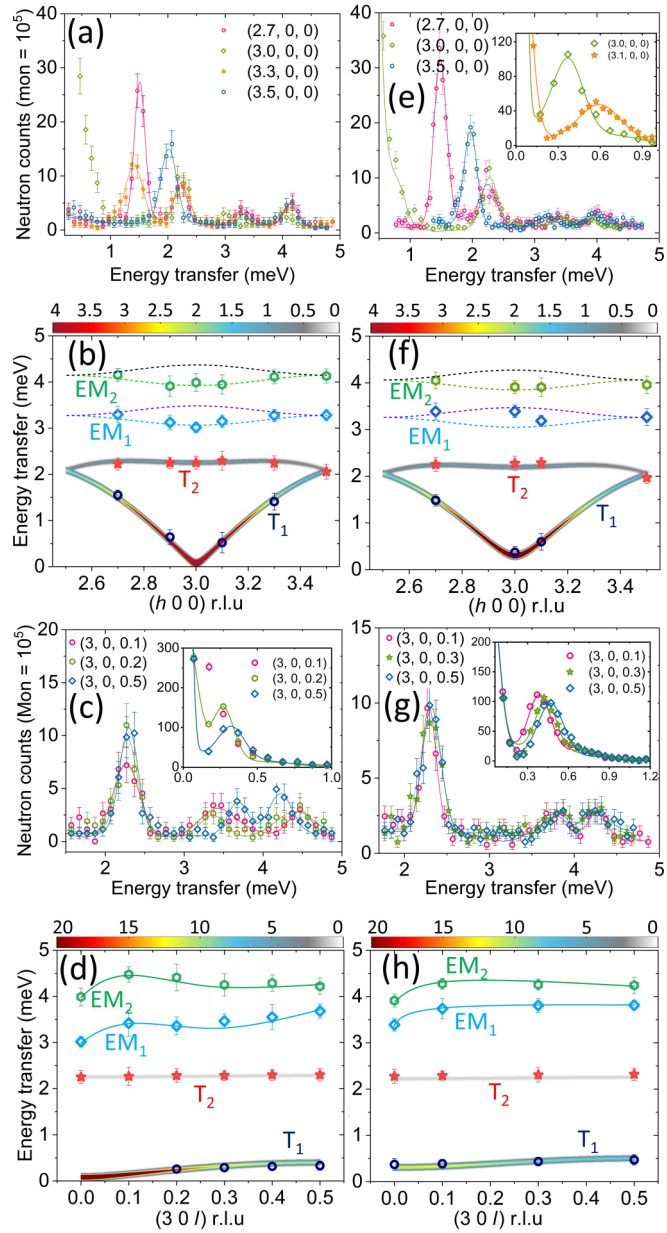

FIG. 2. Three-dimensional spin dispersion at magnetic fields of 0 T (left column) and 2 T (right column). (a), (e) In-plane and (c), (g) out-of-plane constant-Q scans and the corresponding calculated spin dispersion displayed in (b), (f) and (d), (h), respectively, with the overplotted dispersion points (ω, k). Only the solid lines in (d) and (h) are guides for the eye to the EM modes. The zoom sections in (e), (c), and (g) represent the strong acoustic T_1 mode. All the vertical bars in (a)–(h) represent the corresponding error bars.

of the T_1 mode along (h00), which indicates the anisotropic nature of the 3D spin dispersion in $Ba_2CoGe_2O_7$. Please note that the intensity of the T_1 mode along the l direction is ≈10 times the T_2 mode when h = odd [see Figs. 2(c), 2(d), 2(g), and 2(h)] and it should be ≈ 0.1 times when h = even, confirmed by our calculation based on linear spin-wave theory (LSWT). Nonetheless, an interesting feature is that the T_1 mode along l is stronger than the T_1 mode along h, which suggests the transverse in-plane spin fluctuations along the l and h directions are anisotropic too. Here, the T_2 mode is

actually a largely gapped mode (∼2.25 meV) due to the strong SIA effect.

We have validated the observed conventional magnon modes in $Ba_2CoGe_2O_7$ under magnetic fields using the LSWT-based calculation via the SPINW code [24] considering the spin Hamiltonian given below,

$$\mathcal{H} = J\sum_{i,j}\left(S_i^x S_j^x + S_i^y S_j^y + \Delta S_i^z S_j^z\right) + J'\sum_{i,j}(\mathbf{S}_i\cdot\mathbf{S}_j) + \Lambda\sum_i\left(S_i^z\right)^2 + \sum_{i,j}\mathbf{D}_{i,j}\cdot(\mathbf{S}_i\times\mathbf{S}_j) - \sum_i g\mu_B\mathbf{H}^{\rm ex}\cdot\mathbf{S}_i, \quad (1)$$

where i,j denotes neighboring Co^{2+} spin pairs. Even though the first term in the Hamiltonian represents the anisotropic Ising-type ($\Delta > 1$) exchange interaction, the leading axial easy-plane-type SIA ($\Lambda \gg J\Delta$) term energetically favors the spin to lie on the a-b plane after competing with the DM interaction, favoring a commensurate sublattice AFM ordering of the spins [19,25], while J' (<0) is the weak FM interaction along the c axis [14,22]. The triple product represents the antisymmetric DM interaction and the last term is the Zeeman interaction. The staggered DM component in a closed loop (cl) inside the magnetic unit cell $\sum_{\rm cl} D_{ij(c)} = 0$, indicated as circular arrows in Fig. 1(a), gives an unfrustrated condition of D_c but not for $D_{\rm ab}$. In the presence of a magnetic field ($H^{\rm ex}$), the canting angle between the two sublattice spins is controlled by both the field and the DM interaction, and the energy gap of the T_1 mode at the zone center depends mainly on the field strength as it dominates the U(1) explicit symmetry breaking; see Figs. 2(e)–2(h). All the scans presented in Fig. 2 were fitted with simple Gaussian peak profiles without any background subtraction and we have achieved an excellent agreement between the experimental observation and the calculation.

To directly observe the effects of the SIA under magnetic fields, low-energy INS spectra at the AFM zone center (300) were measured up to 5 meV, as shown in Figs. 3(a)–3(d), along with the simulated dispersions in Figs. 3(e)–3(h). With increasing field, the gap of the T_1 (T_2) mode continues to increase (decrease) and finally gets overlapped at a certain critical field (H_c). Both experimentally and theoretically, we find $H_c \approx 9.5$ T [see Fig. 3(k) and inset of Fig. 3(g)]. With further increasing the field, a complete mode crossing takes place, e.g., at $H = 12$ T [Figs. 3(d) and 3(h)]. Most likely, at $H_c \approx 9.5$ T, the effective anisotropy is not strong enough to compete the Zeeman interaction and, therefore, an anomaly in the magnetization curve occurs and the induced c component of the electric polarization (P_c) starts to decrease at H_c, which have been experimentally observed in Refs. [12–14]. Next we show that such competition results in a tunable SIA constant under fields. However, the obtained and calculated field-dependent intensities (normalized with respect to the magnetic Bragg peak) of the zone-center modes are plotted in Fig. 3(i), with the inset showing a typical Q-dependence intensity fall at 0 T.

Let us begin with the study of the unconventional EM modes under fields. The zone-center electromagnon ($EM_{1,2}$) modes are plotted as a contour map in Fig. 3(j). Here, instead

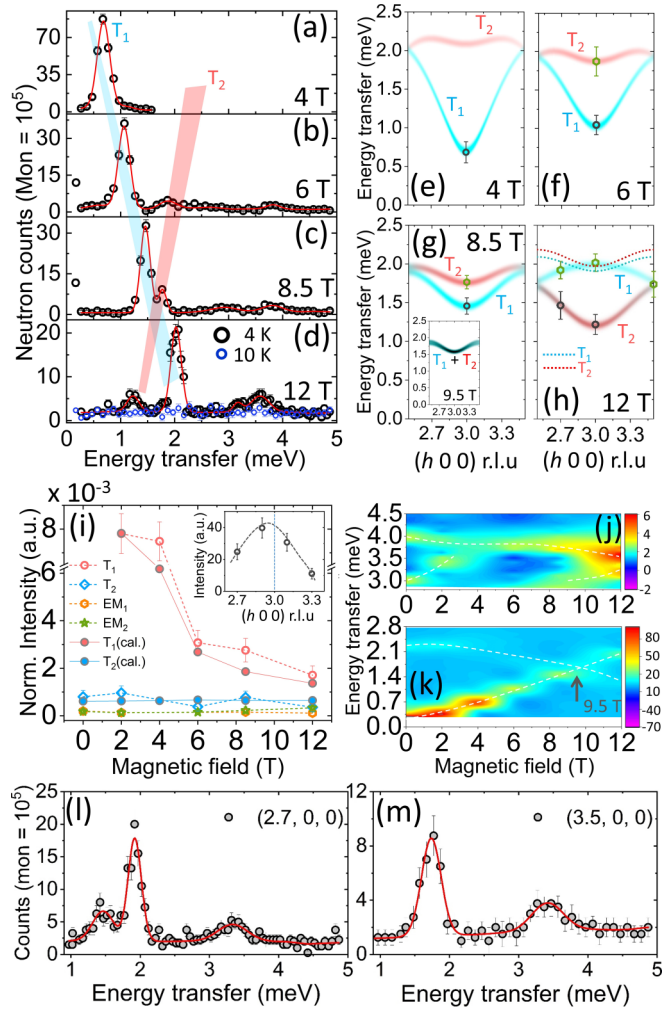

FIG. 3. (a)–(d) Zone-center magnetic excitations at (300) under magnetic fields from 4 to 12 T at 4 K. Only the Bose factor correction was performed on the constant-Q scan at 10 K in (d) and the unit of the y axis for this is χ'' in a.u. Highlighted red and light-cyan shedding corresponds to the T_1 and T_2 mode evolution with fields. (e)–(h) The calculated spin dispersion overplotted with dynamical wave vectors under magnetic fields. The inset in (g) represents the calculated spin waves at 9.5 T. Only the dotted dispersion curve using the fixed SIA (0.75 meV) at 12 T has been overplotted in (h). (i) Intensities of T_1, T_2 and electromagnon ($EM_{1,2}$) modes at (300) under magnetic fields. (j), (k) Contour plots of $EM_{1,2}$ and conventional magnon modes obtained from experimental constant-Q scans at (300), where the arrow indicates the overlapped region and white dashes are a guide for the eye to the modes. (l), (m) Constant-Q scans at 12 T. All the vertical bars in (a)–(m) represent the corresponding error bars.

of the one EM mode reported to date, we have observed two EM modes experimentally in the INS spectra. Also, such two EM modes have been predicted theoretically by Miyahara *et al.* [26] via an exact diagonalization on a 12-site clusters calculation and by Romhányi *et al.* [27] via multiboson spin-wave theory. These EM modes are not captured by our LSWT calculation as the higher-order spin interaction terms are not implemented. Nevertheless, to describe the dispersive nature of the EM modes under magnetic fields, we have used the

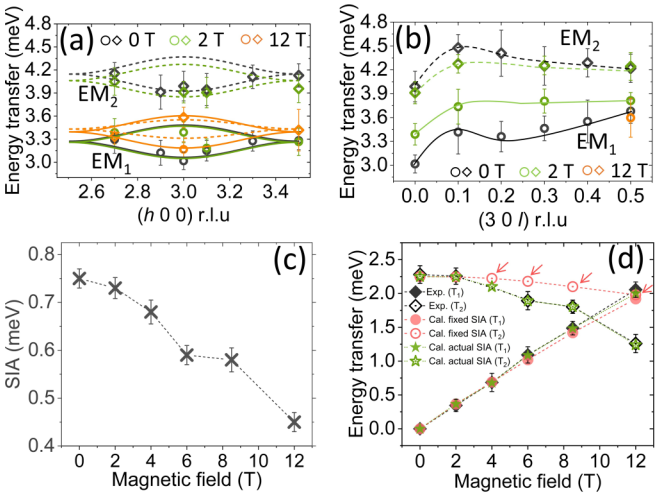

FIG. 4. Evolution of (a) in-plane and (b) out-of-plane electromagnon modes under magnetic fields. In (a), the solid and dashed lines are calculated dispersion curves, while in (b), they are guide lines (not calculated). The solid line and open circles correspond to the EM_1 mode, while the dashed line and open diamonds are for the EM_2 mode. (c) Values of SIA constants under external magnetic fields. (d) Energy values of the magnetic-field-dependent T_1 and T_2 modes obtained via experiment and calculations: experimentally observed (black), calculated while keeping the zero-field SIA constant ($\Lambda = 0.75$ meV) fixed (red), and calculated using the actual SIA constants taken from (c) (green). Red arrows indicate highly deviated T_2 modes (red open circles) from experiment (green open stars). All the vertical bars in (a)–(d) represent the corresponding error bars.

solutions of the effective Hamiltonian proposed by Penc *et al.* [17] and Romhányi *et al.* [27] in the frame of a multiboson theory for the in-plane spin stretching modes in $Ba_2CoGe_2O_7$. Even though DM interactions were not included in the reported zero-field multiboson dispersion relations $\omega_{c,d}(k)$ for EM modes, we could almost explain the observed EM dispersive nature along (h00) after considering variable SIA constants and higher-order terms [see Fig. 4(a)]. Only the lower branches of the $EM_{1,2}$ modes have been observed and they agree nicely with the calculated $\omega_{c,d}(k)$ dispersion relations. These EM modes are suggested to be sensitive to the spin stretching amplitude [17] and the equivalent *d-p* hybridized antiferroelectric constant, i.e., spin nematic interaction [18]. Interestingly, we find that they are dependent on the SIA; in other words, on the external magnetic fields as well. As shown in Figs. 4(a) and 4(b), the EM_1 modes seem to be quite robust at 0 and 2 T, while at 12 T the EM_2 modes shift to the lower energy near the EM_1 mode. We believe that the changes in the SIA constant under fields are responsible for this phenomena since the antiferroelectric constant from the *d-p* hybridization coupling might be sensitive to the applied electric and magnetic field via the crystal electric field (CEF) effect and also under external pressure [11].

To extract the strength of the exchange interactions ($J = 0.207$, $J' = -0.0052$ meV and $\Delta = 1.18$), the DM interactions ($D_{ab} = 0.015$, $D_c = \pm 0.0103$ meV), and the SIA constant ($\Lambda_{H=0} = 0.75$ meV), we have performed the refinement of the INS spectrum using the SPINW code. Slight anisotropic g tensors have been incorporated in the Hamiltonian at higher fields to adjust the gap in the T_1 mode. Similarly, after careful inspection of the energy value of the T_2 mode at (300) presented in Fig. 2 and Figs. 3(a)–3(h), we have noticed that the changes in its energy value are mainly dependent on the changes in the SIA constant being independent of other interactions. Of course, the SIA affects the T_2 mode over whole Q range, but the most dominant change occurs at the zone center (300) while these T_2 modes in the THz spectrum are barely visible to determine the SIA effect. It is worthwhile to mention that the size of the SIA constant in this present study at 4 K is slight smaller than the value reported in Refs. [16,18] at 1.5 K. The reason for this deviation could be the different measurement temperatures. Such decrease in the SIA constant with temperature has been observed as well in other multiferroic antiferromagnets such as $BiFeO_3$ [28] and $HoMnO_3$ [29]. However, the value of the SIA constant and its effect mainly on the T_2 mode under applied magnetic fields are presented in Figs. 4(c) and 4(d). The fixed value of the zero-field SIA constant does not give a good agreement with the experimental observation for the fields above 2 T, and it also shows that the mode crossing takes place at an incorrect field near 12 T. We have confirmed via simulations that this change in energy level of T_2 can only be reproduced by varying the strength of the SIA constant, not that of J or the DM interaction. Since the difference between considering fixed or actual SIA is much more pronounced for the T_2 mode, we have presented the simulated dispersion curve with the fixed SIA in Fig. 3(h) and two extra constant-Q scans are shown in Figs. 3(l) and 3(m) to deliver the confidence on the calculation using actual SIA. Thus, we conclude that the SIA constant gets tuned under a magnetic field and, therefore, affects the T_2 and the EM modes, which are remarkable findings in the physics of multiferroic quantum SLHAF materials.

From the theoretical aspect, in the absence of the DM interaction and field, the AFM quantization axis is chosen arbitrarily where spontaneous rotational symmetry U(1) breaking gives rise to a Goldstone mode. But under an applied magnetic field, the induced canting angle ($\delta\varphi$) between the sublattice spins in the magnetic ground state is no longer arbitrary, keeping the order parameter (η) unchanged until the onset of saturation magnetization and giving rise to a gap for the T_1 mode. In the Hamiltonian, the Zeeman term is quite strong as the SIA term, e.g., a magnetic field of 6 T has the same order of magnitude in energy ($g\mu_B H \approx 0.69$ meV) as the SIA constant, and a competition could take place between them since the transverse field itself forces the spins to be planer and quantized along its direction. On the other hand, the magnetic field can mediate the magnetic anisotropy via CEF and spin-orbit coupling (SOC). In the $3d^n$ transition metal ions, the CEF effects are stronger than SOC, but a comparable SOC leaves the orbital moment unquenched and introduces an extra orbital splitting in addition to those CEF splittings, modifying the magnetic anisotropy. Such unquenched orbital angular momentum [30] under rotations of the magnetic field and also the toroidal moment [31] have been found in $Ba_2CoGe_2O_7$, which confirms the presence of the SOC effect. Since the magnetic field induces a local electric field in the tetrahedral metal-ligand (CoO_4) environment (because of its multiferroic properties), CEF and SOC

coupling both act accordingly with that and might result in tuning of the magnetic anisotropy. Such microscopic origin of the SIA changes could perhaps be better studied by means of detailed CEF excitation energy levels under magnetic fields and considering the CEF parameters and intermediate SOC coupling as perturbation into the effective Hamiltonian, allowing precise determination of the CEF parameters (B_n^m) and construction of detailed maps of magnetic and g anisotropy to be studied.

In summary, our study reveals three-dimensional anisotropic spin excitations in the multiferroic antiferromagnet $Ba_2CoGe_2O_7$, under applied magnetic fields up to 12 T at 4 K. In fact, in contrast to conventional magnons, the INS spectrum shows the existence of two unconventional electromagnon modes which are also dispersive in 3D and responsive to the external magnetic field. Most strikingly, the external magnetic field leads to a tunable axial easy-plane-type SIA, which is a remarkable finding as it also gives a hint to have possible similar effects in the presence of an external electric field. In particular, all the conventional spin-wave modes under magnetic fields are in good accordance with the calculated spin dispersion via LSWT considering a spin-3/2 model Hamiltonian. Nevertheless, this study provides insight into a complex intercorrelation among the SIA, the DM interaction, and the external magnetic field in SLHAF materials leading to many interesting key features such as mode crossing and an anisotropy spin gap of the T_1 and T_2 modes. Our study encourages the further search for multiferroic devices where the tuning of SIA either via an electric or magnetic field is possible and investigation of the dynamical aspects where the SIA is less dominant and spins are noncollinear, such as in its sister compound $Ba_2Cu_{1-x}M_xGe_2O_7$ (M = Co, Mn).

We thank Professor I. Kézsmárki for the fruitful discussions. We thank the technician team for helping us with the cryomagnet at PANDA. R.D. and V.H. would like to acknowledge the support from the Institut für Kristallographie, RWTH Aachen Universität and Jülich Centre for Neutron Science at Heinz Maier-Leibnitz Zentrum.

[1] S. Chakravarty, B. I. Halperin, and D. R. Nelson, Phys. Rev. B **39**, 2344 (1989).
[2] Zheng Weihong, R. H. McKenzie, and R. R. P. Singh, Phys. Rev. B **59**, 14367 (1999).
[3] W. Selke, G. Bannasch, M. Holtscheider, I. P. McCulloch, D. Peters, and S. Wessel, Condens. Matter Phys. **12**, 547 (2009).
[4] J. Romhányi, F. Pollmann, and K. Penc, Phys. Rev. B **84**, 184427 (2011).
[5] S. Kar, K. Wierschem, and P. Sengupta, Phys. Rev. B **96**, 045126 (2017).
[6] D. C. Johnston, Phys. Rev. B **95**, 094421 (2017).
[7] Z. L. Li, J. H. Yang, G. H. Chen, M.-H. Whangbo, H. J. Xiang, and X. G. Gong, Phys. Rev. B **85**, 054426 (2012).
[8] T. Goswami and A. Misra, Chem. Eur. J. **20**, 13951 (2014).
[9] P. Fröbrich, P. J. Jensen, and P. J. Kuntz, Eur. Phys. J. B **13**, 477 (2000).
[10] J. Romhányi, M. Lajkó, and K. Penc, Phys. Rev. B **84**, 224419 (2011).
[11] T. Nakajima, Y. Tokunaga, V. Kocsis, Y. Taguchi, Y. Tokura, and T. H. Arima, Phys. Rev. Lett. **114**, 067201 (2015).
[12] V. Hutanu, A. P. Sazonov, M. Meven, G. Roth, A. Gukasov, H. Murakawa, Y. Tokura, D. Szaller, S. Bordács, I. Kézsmárki, V. K. Guduru, L. C. J. M. Peters, U. Zeitler, J. Romhányi, and B. Náfrádi, Phys. Rev. B **89**, 064403 (2014).
[13] H. Murakawa, Y. Onose, S. Miyahara, N. Furukawa, and Y. Tokura, Phys. Rev. Lett. **105**, 137202 (2010).
[14] H. Murakawa, Y. Onose, S. Miyahara, N. Furukawa, and Y. Tokura, Phys. Rev. B **85**, 174106 (2012).
[15] M. Soda, S. Hayashida, B. Roessli, M. Månsson, J. S. White, M. Matsumoto, R. Shiina, and T. Masuda, Phys. Rev. B **94**, 094418 (2016).
[16] M. Soda, L. J. Chang, M. Matsumoto, V. O. Garlea, B. Roessli, J. S. White, H. Kawano-Furukawa, and T. Masuda, Phys. Rev. B **97**, 214437 (2018).
[17] K. Penc, J. Romhányi, T. Rõom, U. Nagel, A. Antal, T. Fehér, A. Jánossy, H. Engelkamp, H. Murakawa, Y. Tokura, D. Szaller, S. Bordács, and I. Kézsmárki, Phys. Rev. Lett. **108**, 257203 (2012).
[18] M. Soda, M. Matsumoto, M. Månsson, S. Ohira-Kawamura, K. Nakajima, R. Shiina, and T. Masuda, Phys. Rev. Lett. **112**, 127205 (2014).
[19] A. Zheludev, T. Sato, T. Masuda, K. Uchinokura, G. Shirane, and B. Roessli, Phys. Rev. B **68**, 024428 (2003).
[20] S. Bordács, I. Kézsmárki, D. Szaller, L. Demkó, N. Kida, H. Murakawa, Y. Onose, R. Shimano, T. Rõom, U. Nagel, S. Miyahara, N. Furukawa, and Y. Tokura, Nat. Phys. **8**, 734 (2012).
[21] V. Hutanu, A. Sazonov, H. Murakawa, Y. Tokura, B. Náfrádi, and D. Chernyshov, Phys. Rev. B **84**, 212101 (2011).
[22] V. Hutanu, A. Sazonov, M. Meven, H. Murakawa, Y. Tokura, S. Bordács, I. Kézsmárki, and B. Náfrádi, Phys. Rev. B **86**, 104401 (2012).
[23] A. Schneidewind and P. Čermák, J. Large-Scale Res. Fac. **1**, A12 (2015).
[24] S. Toth and B. Lake, J. Phys.: Condens. Matter **27**, 166002 (2015).
[25] T. Sato, T. Masuda, and K. Uchinokura, Phys. B: Condens. Matter **329**, 880 (2003).
[26] S. Miyahara and N. Furukawa, J. Phys. Soc. Jpn. **80**, 073708 (2011).
[27] J. Romhányi and K. Penc, Phys. Rev. B **86**, 174428 (2012).
[28] J. Jeong, M. D. Le, P. Bourges, S. Petit, S. Furukawa, S.-A. Kim, S. Lee, S.-W. Cheong, and J.-G. Park, Phys. Rev. Lett. **113**, 107202 (2014).
[29] O. P. Vajk, M. Kenzelmann, J. W. Lynn, S. B. Kim, and S.-W. Cheong, J. Appl. Phys. **99**, 08E301 (2006).
[30] I. V. Solovyev, Phys. Rev. B **91**, 224423 (2015).
[31] P. Toledano, D. D. Khalyavin, and L. C. Chapon, Phys. Rev. B **84**, 094421 (2011).